Biosensors and Bioelectronics 142 (2019) 111507

Contents lists available at ScienceDirect

Biosensors and Bioelectronics

journal homepage: www.elsevier.com/locate/bios

Integration of diagnosis and treatment in the detection and kill of *S.aureus* in the whole blood

Tingting Xu[a], Jiming Li[a], Shaoyin Zhang[a], Yongcan Jin[a,*], Rui Wang[b,**]

[a] Jiangsu Province Key Laboratory of Pulp and Paper Science and Technology, College of Light Industry and Food Engineering, Nanjing Forestry University, Nanjing, 210037, China

[b] State Key Laboratory of Materials-Oriented Chemical Engineering, College of Food Science and Light Industry, Nanjing Tech University, Nanjing, 211816, China

ARTICLE INFO

Keywords:
S.aureus
Integration of diagnosis and treatment
Electrochemical immunosensor
Hyaluronic acid
MMSNs

ABSTRACT

Fast and accurate detection of *S. aureus* and effectively kill *S. aureus* in the bloodstream in low doses acted as key roles in medicine and microbiology studies. In this work, sufonated-hyaluronic acid (S-HA) terminated magnetic mesoporous silica nanoparticles (MMSNs) loaded with vancomycin was successfully prepared, and *S. aureus* antibody was further modified on the surface of MMSNs (Ab@S-HA@MMSNs) by amidation reaction. The result showed that Ab@S-HA@MMSNs were 240 nm-sized spheres with worm-like mesoporous channels. With the aid of magnetic interaction, Ab@S-HA@MMSNs were modified on the surface of magnetic glassy carbon electrode (MGCE). This prepared immunosensor exhibited an excellent detection limit and linear range, and possessed good selectivity, stability and reproducibility. Besides, since the S-HA terminated MMSNs have anticoagulant property, the Ab@S-HA@MMSNs/MGCE showed antiadhesion property, which ensure that it can be directly applied to detect the amount of *S. aureus* in whole blood. What's more, with an increasing amount of *S. aureus* arriving at MGCE, the capping Ab@S-HA@MMSNs were degraded by Hyal which was secreted by *S. aureus*, and the packaged vancomycin was subsequently released. Ultimately, *S. aureus* can be effectively killed. Therefore, this integrated platform would be a promising multifunctional platform for achieving accurate diagnosis and efficient treatment of *S. aureus* bloodstream infection.

1. Introduction

Staphylococcus aureus (S.aureus), a Gram-positive bacterium, is one of the most important pathogenic bacteria. And *S. aureus* bloodstream infection, which is also known as bacteraemia, is one of the most extensive and serious bacterial infections worldwide (Thammavongsa et al., 2015). Previous studiesreported that bloodstream infections and sepsis have better outcomes when effective antimicrobial therapy is administered early (Dubourg et al., 2018). And data displayed that each hour of delay over 6 h following septic shock in antibiotic administration decreases the survival rate of more than 7% (Ferrer et al., 2014). Hence, fast and accurate detection of *S. aureus* and effectively killing the *S. aureus* in the bloodstream in low doses are crucial and act as key roles in medicine and microbiology studies.

Integrating diagnosis and treatment to achieve accurate diagnosis and efficient treatment of diseases has always been an important goal of modern medicine (Mura and Couvreur, 2012). In recent years, various imaging methods combined with chemotherapy, thermotherapy, photodynamic therapy and other cancer treatment methods to construct the integration of diagnosis and treatment of tumors have received extensive attention from researchers (Li et al., 2018; Zheng et al., 2018a). This method can not only improve the ability to recognize malignant tumors, but also effectively improve the effect of tumor treatment. Inspired by this, we tried to use the integration of diagnosis and treatment in the detection and kill of *S. aureus* in the whole blood.

The traditional methods for detection and determination of bacterias include culture and plate counting of colony, biochemical and metabolic tests, ELISA, PCR and so on (Cooksey et al., 2019; Bu et al., 2019; Rubab et al., 2018). Most of these approaches hold the drawbacks of consuming lots of manpower, time and equipments, which limited their widespread use. Combining the advantages of high sensitivity, easy miniaturization and can be detected in complex systems, a biosensor has been introduced here (Ranjbar and Shahrokhian, 2018).

In recent years, magnetic mesoporous silica nanoparticles (MMSNs) have been recognized as high-efficiency drug delivery materials due to their good biocompatibility, dispersity, magnetic properties,

* Corresponding author.
** Corresponding author.
E-mail addresses: jinyongcan@njfu.edu.cn (Y. Jin), ruiwang2013@njtech.edu.cn (R. Wang).

https://doi.org/10.1016/j.bios.2019.111507
Received 5 May 2019; Received in revised form 28 June 2019; Accepted 12 July 2019
Available online 13 July 2019
0956-5663/

hydrophilicity, surface paintability and large pore volume (Ni et al., 2017). The drugs can be loaded in the open pores and encapsulated by the degradable molecules which responding to the targeted site microenvironment. And the functional molecules can be further modified on the surface of MMSNs. What's more, due to the excellent magnetic property of MMSNs, they can also be easily modified on the surface of electrode, so as to provide possibility for the integration of diagnosis and treatment (Yuan et al., 2016). In this way, an "on-demand" integrated platform for diagnosis and treatment towards *S. aureus* has been costructed.

Hyaluronic acid (HA), a kind of acid mucopolysaccharide, is well known for its biocompatibility and water retention (Neto et al., 2014). Since HA can be high-efficiency degraded by hyaluronidase (Hyal), it has been widely used as the targeting and capping agent (Ji et al., 2016). According to the previous literature, many kinds of bacteria were found to be capable of generating Hyal (Tucking et al., 2018). Take advantages of this, HA can be used as a capping agent in response to Hyal presented at bacteria infectious microenvironment. In addition, combining the highly hydrophilic property and vast negative charges caused by a relatively high number of carboxyl groups in HA, it can reduce the platelet adhesion on the surface of materials. Moreover, after sulfonation of HA, the number of platelets adhered on the surface of materials will be further reduced due to the high density of negatives in the inserted sulfonicacid groups (Barbucci et al., 1998). Based on the above, here sulfonated-HA (S-HA) was selected as an ideal capping agent modified on the magnetic mesoporous material to fully exert its target, drug sustained release and anti-adhesion effects.

In this study, a sufonated-HA terminated MMSNs loaded with vancomycin (van) was successfully prepared, and *S. aureus* antibody was further modified on the surface of MMSNs (Ab@S-HA@MMSNs) by amidation reaction. The Ab@S-HA@MMSNs were modified on the surface of magnetic glassy carbon electrode (MGCE) by magnetic interaction (Ab@S-HA@MMSNs/MGCE). By analyzing the change of electrochemical signals which was caused by specific antigen-antibody binding between *S. aureus* in solution and antibody modified on the MGCE, the amount of *S. aureus* in solution can be accurately detected. Besides, since the sufonated-HA terminated MMSNs have anticoagulant property, the MGCE which was modified by Ab@S-HA@MMSNs showed antiadhesion property. Therefore, Ab@S-HA@MMSNs/MGCE can be directly applied to detect the amount of *S. aureus* in whole blood. What's more, with the increase of amount of *S. aureus* arriving at MGCE, the capping Ab@S-HA@MMSNs were degraded by Hyal which was secreted by *S. aureus*, and the packaged van was subsequently released. Ultimately, *S. aureus* can be effectively killed (Scheme 1).

2. Materials and methods

2.1. Materials

Ferric chloride hexahydrate ($FeCl_3{\cdot}6H_2O$), glycol, sodium acetate trihydrate ($NaAc{\cdot}3H_2O$), sodium citrate ($C_6H_8O_7{\cdot}3Na$), N-cetyltrimethylammonium bromide (CTAB), tetraethylorthosilicate (TEOS), dimethylforma-mide (DMF), (3-aminopropyl) trimethoxysilane (APTES), methylbenzene, pyridine, triethylamine, sodium hydroxide (NaOH), potassium ferricyanide (K_3 [$Fe(CN)_6$]), potassium ferrocyanide ($K_4Fe(CN)_6{\cdot}3H_2O$) and ethanol were provided by Sinopharm Chemical Reagent (Shanghai, China). N-hydroxysuccinimide (NHS), 1-Ethyl-3 (3-dimethylaminopropyl) carbodiimide (EDC) and sodium pyridine-3-sulfonate were obtained from Aladdin Reagent (Shanghai, China). Sodium hyaluronate was purchased from Xi'an Zebang Biological Technology Co., Ltd (Xi'an, China). Vancomycin hydrochloride (van) was received from Shanghai Yuanye Biological Technology Co., Ltd (Shanghai, China). Triethanolamine was obtained from Rhawn Reagent (Shanghai, China). All solutions were prepared by Ultrapure water (18.2 MΩ, Milli-Q, Millipore).

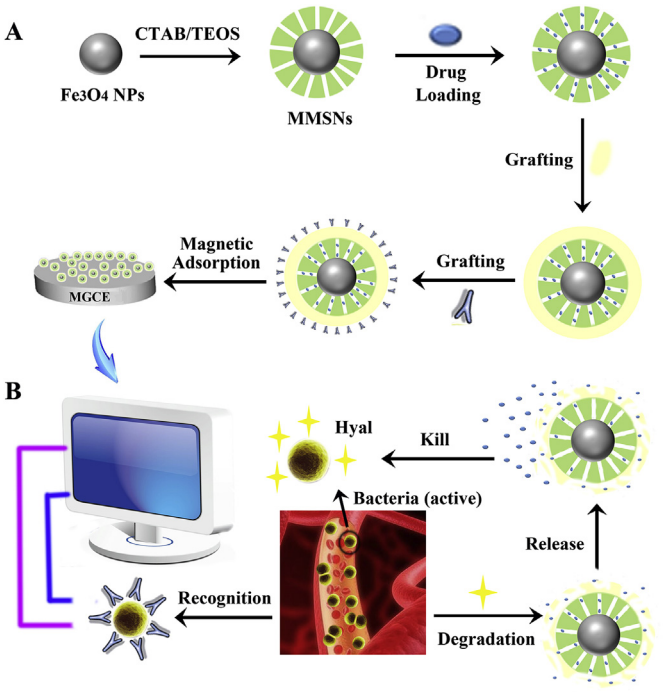

Scheme 1. (A) Preparation of an "on-demand" integrated platform for diagnosis and treatment towards *S. aureus*. (B) Schematic representation of the on-demand drug delivery triggered by bacterial Hyal to inactive *S. aureus* and electrochemical detection of *S. aureus*.

2.2. Preparation of MMSNs

The MMSNs were prepared by two steps according to previous reports. Firstly, magnetic nanocore was synthesized directly through a traditional hydrothermal method (Cao et al., 2008). In detail, $FeCl_3{\cdot}6H_2O$ (1.35 g, 5 mmol), NaOH (0.6 g, 15 mmol), and PEG 10000 (1 g) were completely dissolved in EG (40 mL). Then the mixture solution was transferred into a teflon-lined stainless-steel autoclave and heated to 200 °C. After reaction for 8 h, the oven was cooled to room temperature. The black mixture was washed several times with water and ethanol, followed by being collected with a magnet. Finally, the magnetic nanocore was dried at 60 °C for 24 h under vacuum. Secondly, silica shell was prepared by in-situ hydrolysis of TEOS (Yao et al., 2017). Typically, 0.2 g of magnetic nanocore was dispersed in 60 mL of water under ultrasonication for 30 min. Then 0.6836 g of CTAB and 0.4 g of triethylamine were added into the suspension at 90 °C. After continuous mechanical stirring for 30 min, 2 mL of TEOS was added dropwise into the suspension. After another reaction for 2 h, the brown mixture was washed several times with water and ethanol, followed by being collected with a magnet and dried at 60 °C for 24 h under vacuum. Finally, the MMSNs was obtained by calcination of the dried nanoparticles at 550 °C for 6 h to remove the surfactant.

2.3. Amination of MMSNs

APTES was used to aminate the MMSNs. 0.5 g of MMSNs was evenly dispersed in 100 mL of methylbenzene at 100 °C. Then 0.75 mL of APTES was added into the suspension and continuously mechanical stirred at 120 °C for 20 h in refluxing. Next, the received brown product was extensively washed with methylbenzene to remove the unreacted APTES. Finally, the amino-functionalized MMSNs was obtained after drying at 60 °C for 24 h under vacuum.

2.4. Sulfonation of HA (S-HA)

Before sulfonation, the –COOH groups were firstly protected by triethylamine. To be specific, 0.5 g of HA was dispersed in 30 mL of DMF. Then 0.2 mL of triethylamine was added into the mixture solution to form the triethylammonium hyaluronate. After reaction for 1 h, triethylammonium hyaluronate was then transferred into another 30 mL of DMF solution. Next, 0.1 g of sodium pyridine-3-sulfonate was added, and the reaction was carried out for 1 h under N_2 at 0 °C. Afterwards, 1 mL of 1 M NaOH was added dropwise into the above mixture solution. Finally, the product was washed with ethanol and drying at 60 °C for 24 h under vacuum.

2.5. Van loading and preparation of Ab@S-HA@MMSNs

100 mg of MMSNs was incubated in 10 mL of PBS buffer solution (10 mM, pH 7.4) which containing 10 mg/mL of van for 24 h. Meanwhile, 0.1 g of S-HA was dissolved in 20 mL of water and activated by EDC and NHS (mole ratio of –COOH:EDC:NHS = 1:1:1) for 12 h. Subsequently, 100 mg of MMSNs which loaded with van and 1 mL of anti-*S. aureus* (200 ng/mL, PBS, pH 7.4) were slowly added into the activated S-HA solution. After reaction at 4 °C for 12 h, the Ab@S-HA@MMSNs was collected by magnetic adsorption and washed with water to rinse the residual EDC, NHS and S-HA. Finally, the Ab@S-HA@MMSNs was lyophilized and kept at 4 °C (Duangkamon and Volkhard, 2015).

2.6. In vitro van release experiments

The as-synthesized van-loaded Ab@S-HA@MMSNs (20 mg) was dispersed in 10 mL PBS buffer (pH = 7.4) with and without Hyal (100 $U{\cdot}mL^{-1}$ and 500 $U{\cdot}mL^{-1}$) at 37 °C. At set intervals, aliquots (500 μL) were taken from the solution and replaced with an equal volume of the new PBS buffer. The release of van was monitored by the characteristic absorption peak of van at 280 nm (Nor et al., 2016).

2.7. Antibacterial performance test

Luria-Bertani broth was used as cluturing nutrient sources. 1 mg/mL of van and Ab@S-HA@MMSNs medium solution were prepared respectively, filtered by 0.22 μm filtration membranes, and then added into the bacterial solution. After being co-incubated at 37 °C for 24 h, the photos were taken for the aqueous dispersion of *S. aureus*. Next, in order to calculate the bacteriostatic efficiencies of *S. aureus*, 100 μL of bacterial solution was absorbed and uniformly coated on the agar plates. After being co-incubated at 37 °C for another 24 h, the plates were photographed and the survival rate of *S. aureus* was calculated. Finally, 200 μL of bacterial suspension was dripped onto the slides, followed by fixed with 2.5% glutaraldehyde solution (5 mL) for 4 h and dehydration using an ethanol series (20%–100%; 30 min), and subsequently freeze-dried. The dried samples were characterized by SEM analysis (Wang et al., 2017).

2.8. Hemolytic assay

Firstly, the fresh whole blood was centrifuged at 1500 rpm for 10 min. Then, the received erythrocytes were washed three times with 10 mL PBS by centrifugation at 2500 rpm for 5 min and resuspended in the same buffer to prepare 2% erythrocytes suspension. Next, 1 mg/mL of Ab@S-HA@MMSNs which had been pre-dispersed in PBS buffer was added to the erythrocytes suspension and incubated in water bath at 37 C. At the same time, distilled water and PBS buffer were set as positive and negative controls respectively. 1 h later, the mixtures were centrifuged at 1500 rpm for 10 min. The absorbance values of the supernatants at 545 nm were recorded. The percent hemolytic of erythrocytes was calculated using the following formula: hemolysis rate (%) = [(ODtest − ODneg)/(ODpos − ODneg)] × 100%. In this formula, ODtest, ODneg, and ODpos were the absorbance of the test sample, negative control (PBS), and positive control (water), respectively. All the hemolysis experiments were performed in triplicate (Liu et al., 2007).

2.9. Morphological changes of erythrocytes

The morphological changes of erythrocytes were examined by a light microscopy (Tong et al., 2013). The erythrocytes suspension was obtained according to the method in hemolysis test. Then 1 mg/mL of Ab@S-HA@MMSNs which had been pre-dispersed in PBS were co-incubated with erythrocytes suspension in a 37 °C water bath for 1 h. The morphological changes of erythrocytes were observed and photographed.

2.10. Whole blood adhesion tests

In order to ensure that Ab@S-HA@MMSNs/MGCE can be directly applied to detect *S. aureus* in the whole blood, the whole blood adhesion tests were carried out (Smith et al., 2010). Firstly, the surface sections of blank substrate and Ab@S-HA@MMSNs modified substrate were balanced in PBS buffer for 24 h in a 24-well microplate. Then 1 mL of the pre-warmed whole blood was added into each well. After incubation for 30 min at 37 °C, substrates were taken out and washed three times with PBS buffer mildly. Next, the substrates were fixed with 2.5% glutaraldehyde of PBS buffer for 30 min to fix the adhered blood cells. Finally, substrates were rinsed three times with PBS buffer and dehydrated with ethanol/water solutions (50, 60, 70, 80, 90, 95 and 100% of ethanol) for 30 min each and air dried. The substrates attached with blood cells were gold deposited in vacuum and examined by scanning electron microscope.

2.11. Preparation of the immunosensor and the electrochemical determination

Before modification, the MGCE was polished sequentially with 0.3 and 0.05 mm aluminum slurries and rinsed thoroughly with double-distilled water to a mirror-like surface. Then, 8.0 μL of 1 mg/mL Ab@S-HA@MMSNs was carefully dropped on the MGCE surface and dried in air at room temperature to obtain a modified MGCE (Ab@S-HA@MMSNs/MGCE). Next, in order to avoid non-specific adsorption, the Ab@S-HA@MMSNs/MGCE was immersed in 5 wt% BSA solution for 1 h at the ambient temperature, followed by being washed with double-distilled water three times. Thus, the immunosensor was obtained. All electrochemical measurements were carried out at room temperature in 5 mM K_3 $[Fe(CN)_6]$ using electrochemical workstation (Shanghai Chenhua, China). The Ab@S-HA@MMSNs/MGCE was acted as working electrode. The electrochemical impedance spectroscopy (EIS) measurements were conducted in the frequency ranging from 1 Hz to 100 kHz with 5 mV AC amplitude. Cyclic voltammetry (CV) was performed over the potentials between −0.4 V and 1 V. Differential pulse voltammetry (DPV) was carried out at 0.05 V with 0.2 s pulse width (Mohammadniaei et al., 2018).

3. Results and discussions

3.1. Preparation of Ab@S-HA@MMSNs

The MMSNs were prepared by two steps according to previous reports. The surfaces modification of MMSNs were carried out by using silane coupling agent KH550. The amino modified MMSNs were incubated in van PBS buffer solution to load van. The S-HA was obtained through the reaction between pyridine sulfonate and –OH groups on HA. For the purpose of prevent the premature leakage of van, S-HA was conjugated on the surface of MMSNs by amidation reaction. The

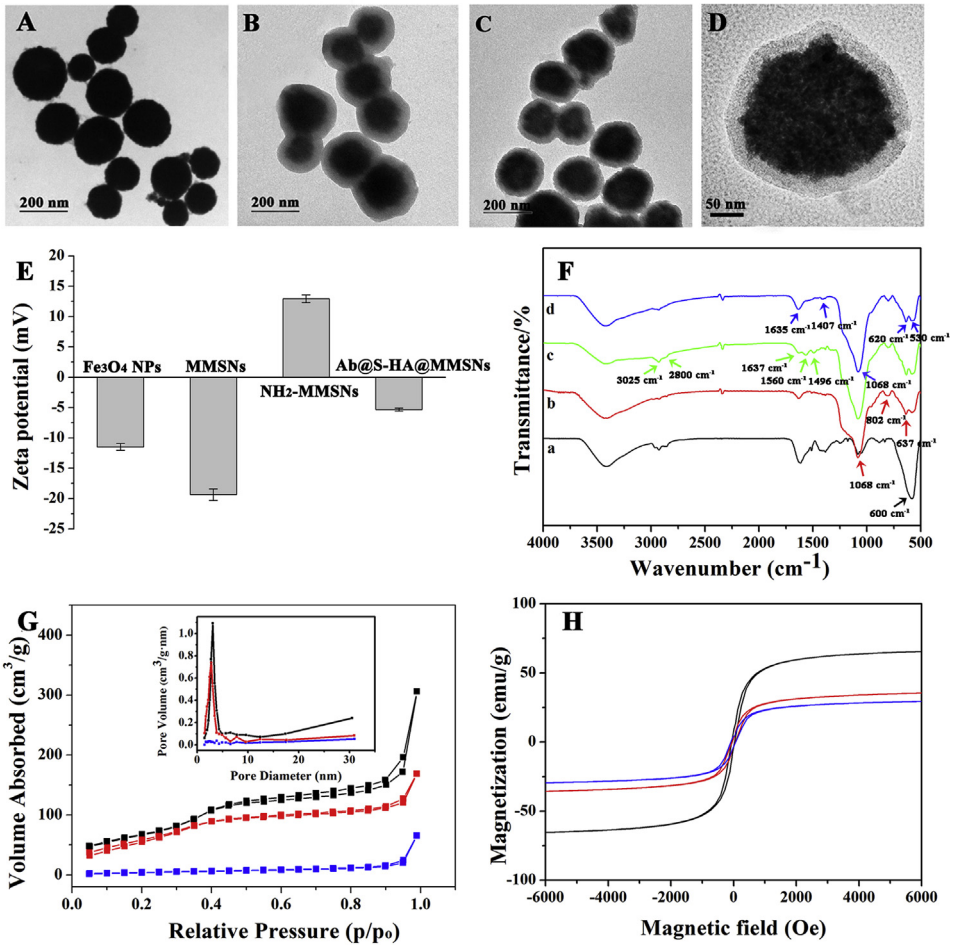

Fig. 1. TEM images of (A) Fe_3O_4 NPs, (B) MMSNs, (C) Ab@S-HA@MMSNs and (D) HRTEM image of Ab@S-HA@MMSNs. (E) Zeta potential and (F) FT-IR spectra of Fe_3O_4 NPs, MMSNs, NH_2-MMSNs and Ab@S-HA@MMSNs. (G) N_2 adsorption-desorption isotherms and pore size distributions and (H) magnetization curves of MMSNs, NH_2-MMSNs and Ab@S-HA@MMSNs.

antibody was finally modified on the surface of S-HA@MMSNs by further amidation reaction.

The sulfonation reaction occurred through a nucleophilic attack of the –OH groups of HA on the S atom of pyridinesulfonate. As shown in X-ray photoelectron spectroscopy (XPS) results, since no S (2p) signal can be detected from amino modified MMSNs, the appearance of the S (2p) core-level signal after sulfonation confirms the success of sulfonation reaction (Fig. S1). According to the previous literatures, the degree of sulfanoation was positively proportional to the amount of added pyridinesulfonate (Cen et al., 2004). And excessive sulfonation modification was not conducive to the degradation of HA by Hyal in the later stage (Abatangelo et al., 1997). Here the molar ratio of –OH and $–SO_3$ were set as 1:0.5.

Transmission electron microscope (TEM) images showed that the average particle size of pure Fe_3O_4 NPs was estimated to be 180 nm (Fig. 1A). After the coating of masoporous silica shell, the particles size was increased to 240 nm (Fig. 1B), and the worm-like mesoporous channels can be clearly observed on the shells. When MMSNs was loaded with van and capped by S-HA and antibody through amidation reaction, the morphology and size of Ab@S-HA@MMSNs did not change obviously compared to MMSNs (Fig. 1C). In the enlarged view, it can be clearly seen that the Ab@S-HA@MMSNs was 180 nm core uniformly wrapped with 30 nm shell (Fig. 1D).

Zeta potential was used to judge whether the sysnthesis of Ab@S-HA@MMSNs was successful. As shown in Fig. 1E, the zeta potential of pure Fe_3O_4 NPs was −11.48 mV. After the coating of masoporous silica shell, the zeta potential changed to −19.36 mV, The reason was the fact that masoporous silica exhibits electronegativity above the isoelectric point (Zheng et al., 2018b). The zeta potential of MMSNs after amino modification changed to 12.93 mV, which can be attributed to the introduce of positive charged amino groups (Xu et al., 2017). When MMSNs was futher loaded with van and capped by S-HA, the zeta potential changed to −5.32 mV because sulfonate was electronegative at neutral pH (Thiangthan et al., 2019). This result indicated that the synthesis of Ab@S-HA@MMSNs was successful.

In order to further analyze the preparation process of Ab@S-HA@MMSNs, fourier transform infrared (FT-IR) spectra and N_2 sorption technique were carried out in this study. As shown on FT-IR spectra (Fig. 1F), the characteristic peaks at around 600 cm^{-1} existing in all curves were attributed to the characteristic absorption of Fe–O in Fe_3O_4 NPs (Han et al., 2019) (curve a). After coating with SiO_2 shell, typical Si–O–Si bands including the symmetric stretching vibration peak at 637 cm^{-1} and 802 cm^{-1} and the deformation vibrations at 1068 cm^{-1} appeared (Cheng et al., 2018) (curve b). Successful aminopropyl modification of MMSNs was also evidenced by the adsorption at 1637 cm^{-1}, 1560 cm^{-1} and 1496 cm^{-1}, which were attributed to the stretching and bending vibrations of amino groups. Besides, the stretching vibration of methylene groups were also appeared between 2800 cm^{-1} and 3025 cm^{-1} (Wang et al., 2010) (curve c). Furthermore, the successful coating of S-HA onto MMSNs was verified by the stretching vibrations at 1407 cm^{-1} and 1635 cm^{-1}, which could be assigned to the C–N and amide C=O groups, respectively (Sun et al., 2018) (curve d). The peaks of sulfonic acid groups appeared at 1068 cm^{-1}, 620 cm^{-1} and 530 cm^{-1} also proved the successful

preparation of Ab@S-HA@MMSNs.

N_2 adsorption-desorption isotherms and pore size distributions of MMSNs, MMSNs after amino modification and Ab@S-HA@MMSNs loaded with van were shown in Fig. 1G. The MMSNs exhibited typical type-IV isotherm, illustrating the MMSNs possessed mesoporous structure (Zhang et al., 2012). The mesopore size, surface area and pore volume of MMSNs were 3.051 nm, 310.60 $m^2 g^{-1}$ and 0.32 $cm^3 g^{-1}$. After being modified with amino groups, the N_2 adsorption amount of MMSNs decreased sharply. And the mesopore size, surface area and pore volume decreased to 2.742 nm, 246.38 $m^2 g^{-1}$ and 0.24 $cm^3 g^{-1}$, respectively, which suggesting the successful modifaction of amino groups. Since the size of van was smaller than 2.742 nm, it can diffuse into the mesoporous channels of MMSNs easily. So after van loading and S-HA capping, the N_2-adsorption amount further decreased. The mesopore size, surface area and pore volume decreased to 1.692 nm, 27.02 $m^2 g^{-1}$ and 0.044 $cm^3 g^{-1}$, which indicates the van loading in mesoporous channels and the capping effect of S-HA (Chi et al., 2018).

Whether Ab@S-HA@MMSNs could be firmly fixed on the MGCE, magnetism was an important indicator. Fig. 1H showed the magnetization curves of Fe_3O_4 NPs, MMSNs and Ab@S-HA@MMSNs measured at 298 K. The saturation magnetization values of Fe_3O_4 NPs, MMSNs and Ab@S-HA@MMSNs were 64.88, 35.03, 29.18 emu/g, respectively. The decrease of saturation magnetization values was attributed to the mixture of lower magnetic components (Yang et al., 2009). The magnetic attraction of Ab@S-HA@MMSNs were tested in distilled water by placing a magnet near the sample bottle. A quick aggregation of Ab@S-HA@MMSNs towards the magnet could be observed within 20 s, demonstrating directly that Ab@S-HA@MMSNs possessed good magnetic responsivity and can be utilized to modify MGCE for the later electrochemical test.

3.2. Loading efficiency and in vitro van release experiments

In order to explore the potential of employing Ab@S-HA@MMSNs as a controlled drug delivery carrier, the loading efficiency of van in Ab@S-HA@MMSNs was calculated. According to the standard curve van absorbance value at 280 nm, the maximum loading ratio of van was calculated to be 10.7 wt %.

The Hyal-activated release of van from Ab@S-HA@MMSNs was discussed in PBS buffer (pH = 7.4). The MMSNs which was not encapsulated with S-HA exhibited sudden van release property. However, for Ab@S-HA@MMSNs, very few van was detected when no Hyal had been added, which avoided the harm caused by the abuse of antibiotics. When the Hyal was added at a concentration of 100 U/mL, van can be released quickly in a short time, and the release can accumulate over 72 h. We believe that the long-term sustained release can avoid drug waste and side effects caused by sudden drug release. When the concentration went up to 500 U/mL, after 48 h, the cumulative release rate tended to be stable, reaching 83%. The obvious difference suggested the important role of Hyal in the “on-demand” drug release (Fig. S2).

3.3. Antibacterial performance test

Given that van can be controlled-released from Ab@S-HA@MMSNs under the action of Hyal, and *S. aureus* was found to be capable of generating Hyal, we believed the Ab@S-HA@MMSNs have antibacterial effects. As the results showed in Fig. 2A, the culture mediums which supplemented with van or Ab@S-HA@MMSNs were clarified after 24 h of incubation with *S. aureus*, while the control medium was very turbid, which suggested that both the pure van and Ab@S-HA@MMSNs possess antibacterial function. Further, the bacteriostatic efficiencies were calculated. The corresponding values of Ab@S-HA@MMSNs can reach up to 98% (Fig. 2B). What's more, the results gotten from plate count test and micromorphological characteristics of bacterials experiment were consistent with above. Compared with the control, the total number of colonies decreased obviously after adding Ab@S-HA@MMSNs (Fig. 2C–D), and surface roughness and bacteria deformation were observed (Fig. 2E–F). Hence, the Ab@S-HA@MMSNs was extremely active against *S. aureus*.

3.4. Blood compatibility evaluation of Ab@S-HA@MMSNs

Considering that the Ab@S-HA@MMSNs would eventually be applied to detection and killing *S. aureus* in the blood environment, blood compatibility have been carefully evaluated. The hemolysis ratio was an important datum to evaluate the blood compatibility of materials (Yu et al., 2011). No significant hemolysis was observed for Ab@S-HA@MMSNs (Fig. 3A–B). Results showed that the extent of hemolysis was concentration-dependent for Ab@S-HA@MMSNs. And when the concentration of Ab@S-HA@MMSNs reached 500 μg/mL, the hemolysis ratio was still less than 5%, which reflecting that Ab@S-HA@MMSNs could be regarded as blood compatibility.

Besides, changes in erythrocyte morphologies after co-incubation of materials with erythrocytes can also reflect the blood compatibility of materials. Generally, normal erythrocyte showed biconcave shape. However, if the erythrocytes are exposed to materials possessing bad biocompatibility or the solution ions balance is broken, erythrocyte became deformed, swollen, and even be damaged. Here, the erythrocytes which be co-incubated with the Ab@S-HA@MMSNs did not show any morphological changes, revealing that Ab@S-HA@MMSNs was blood compatibility (Fig. S3).

3.5. Surface morphology characterization of Ab@S-HA@MMSNs/MGCE

SEM was used to evaluate the surface morphology of Ab@S-HA@MMSNs/MGCE. As the results shown in Figs. S4A–S4B, the bare MGCE had a smooth surface. After being modified with Ab@S-HA@MMSNs, uniform distribution of nanoparticles could be seen on the surface of MGCE. The nanoparticles were spherical with a diameter about 240 nm.

3.6. Anti-biofouling property of Ab@S-HA@MMSNs/MGCE

By comparing the whole blood adhesion of the electrode surface before and after the modified of Ab@S-HA@MMSNs, it can be found from the SEM images that a lot of blood cells and platelets were adhered on the blank electrode substrate while the surface of electrode substrate modified with Ab@S-HA@MMSNs was comparatively clean (Figs. S5A–S5B), which indicating that Ab@S-HA@MMSNs/MGCE can be used for whole blood detection directly (Sun et al., 2013).

3.7. Electrochemical characterization of the immunosensor

Before the formal electrochemical test, a series of experimental conditions including concentration of Ab@S-HA@MMSNs, incubation temperature and incubation time were optimized in Fig. S6, results indicated that the optimized conditions were 2 mg/mL, 37 °C and 50 min, respectively.

With the stepwise assembly of the immunosensor, cyclic voltammetry (CV) and electrochemical impedance spectroscopy (EIS) signals of the electrodes were constantly changing. Fig. 4A displayed the CVs of the bare MGCE (curve a), the Ab@S-HA@MMSNs/MGCE (curve b), the BSA/Ab@S-HA@MMSNs/MGCE (curve c) and the *S. aureus*/BSA/Ab@S-HA@MMSNs/MGCE (curve d) in 0.1 M KCl solution containing 5 mM $Fe(CN)6^{4-/3-}$. The figure suggested that bare MGCE presented a pair of well-defined redox peaks, but the current response at the Ab@S-HA@MMSNs-modified MGCE was decreased a little, which can be attributed to the immobilized nanoparticles acted as insulators blocking the electron transfer between the probe and the MGCE. As expected, the current response was further weakened with the layer modification of the MGCE (Lu et al., 2008). In the terms of EIS, the same results confirmed the results obtained by CVs (Fig. 4B). Comparing with the bare MGCE (curve a), the Ret of MGCEs gradually increased along with the

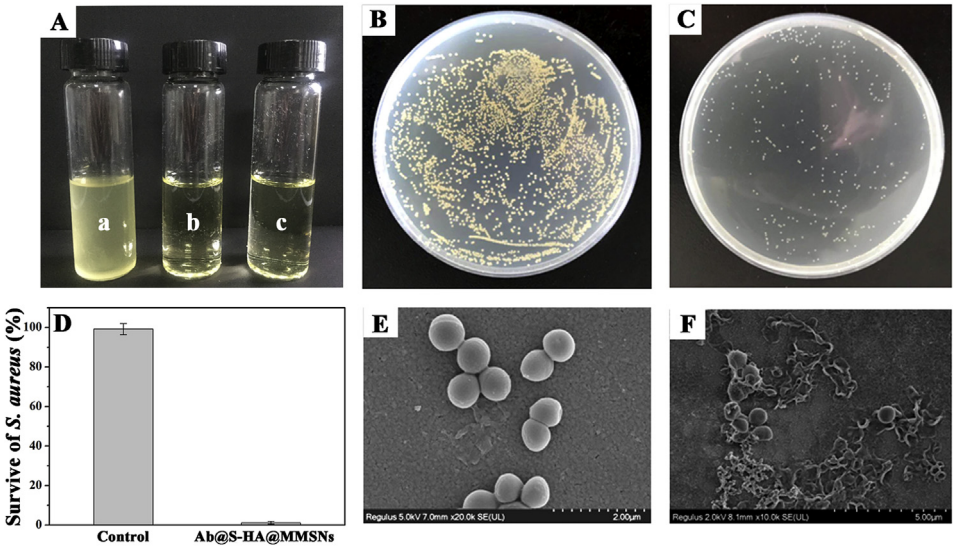

Fig. 2. Antibacterial tests with *S. aureus*. (A) The photos were taken for the aqueous dispersion of *S. aureus* that have been incubated for 24 h in the (a) absence and (c) presence of Ab@S-HA@MMSNs, and (b) in the presence of pure van. (B–C) Then 200 μL of culture solution was plated on the agarized Luria-Bertani medium for another 24 h at 37 °C. (D) Survival rates of *S. aureus* in the absence and presence of Ab@S-HA@MMSNs. SEM images of *S. aureus* (E) before and (F) after exposed to Ab@S-HA@MMSNs.

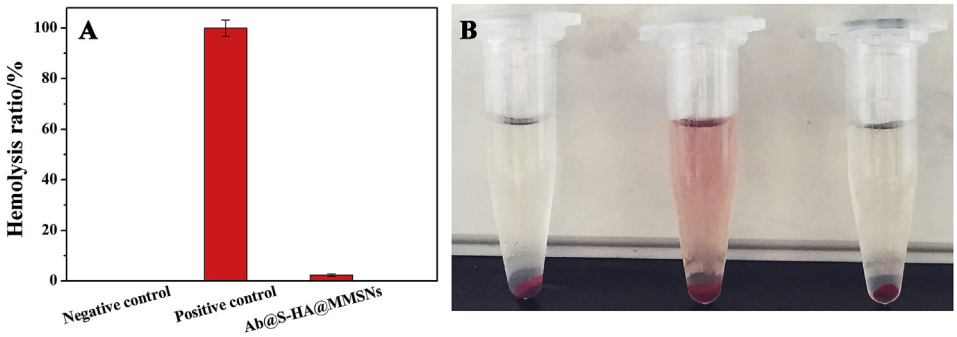

Fig. 3. (A–B) Hemolytic test results of Ab@S-HA@MMSNs.

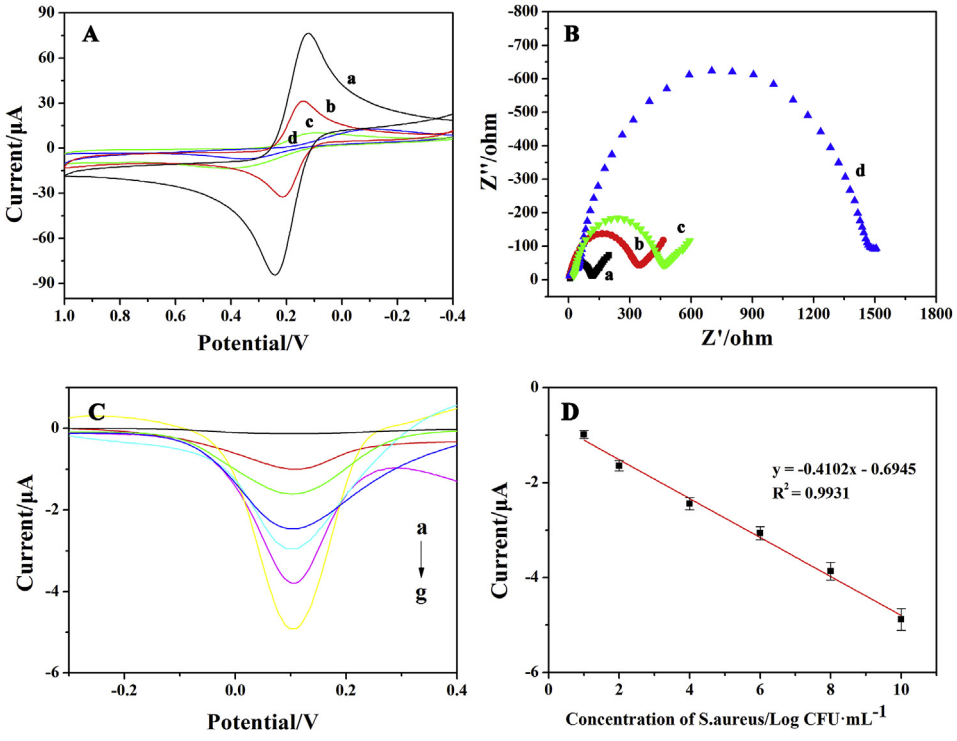

Fig. 4. (A) CVs and (B) EIS spectra of the fabrication progress of the Ab@S-HA@MMSNs modified immune sensor in pH 7.4 PBS containing 0.1 M HCl and 5 mM $Fe(CN)_6^{3-}$/$Fe(CN)_6^{4-}$, (a) bare MGCE, (b) Ab@S-HA@MMSNs/MGCE, (c) BSA/Ab@S-HA@MMSNs/MGCE, and (d) *S. aureus*/BSA/Ab@S-HA@MMSNs/MGCE. (C) DPVs obtained at *S. aureus*/BSA/Ab@S-HA@MMSNs/MGCE with various concentration of *S. aureus* (0, $1*10^1$, $1*10^2$, $1*10^4$, $1*10^6$, $1*10^8$ and $1*10^{10}$ CFU/mL). (D) The calibration curve for *S. aureus* obtained at the *S. aureus*/BSA/Ab@S-HA@MMSNs/MGCE biosensor (RSD ($1*10^1$) = 8.54%; RSD ($1*10^2$) = 6.80%; RSD ($1*10^4$) = 8.54%; RSD ($1*10^6$) = 5.16%; RSD ($1*10^8$) = 4.53%; RSD ($1*10^{10}$) = 4.62%).

Table 1
Comparison of the results obtained by this work with plate counting method.

Samples	Plate counting method (log [*S. aureus* (cfu/ml)])	This work (log [*S. aureus* (cfu/ml)])	Relative deviation (%)
1	3	3.12	8.49
2	5	5.09	6.36
3	7	6.93	4.95

deposition of Ab@S-HA@MMSNs, BSA and *S. aureus*. This was attributed to that the immunocomplex layer on the electrode blocks the electron communication and mass-transfer. Thus, a further increase of the resistance was observed (Guo et al., 2010).

3.8. Analytical performance

The relevance between the concentration of *S. aureus* and peak current was studied under the optimized experimental conditions using differential pulse voltammetry (DPV). The results showed in Fig. 4C–D suggested that with the increase of *S. aureus* concentration from $1*10^1$ CFU/mL to $1*10^{10}$ CFU/mL, the amperometric response decreased. The regression equation was ΔI (10^{-6} A) = -0.4102 logC(CFU/mL)-0.6945 (R^2 = 0.9931). Ten groups of parallel DPV tests for blank samples were conducted to calculate the detection limit. (results shown in Fig. S7). According to the calculation formula: detection limit = 3*Sb/As (Sb is the blank standard deviation and As is the absolute value of slope), the detection limit was calculated to be 3, which indicated that compared with most of the sensors previously developed, this sensor exhibited an excellent detection limit and linear range (Table S1).

Further, the selectivity, stability and reproducibility of the immunosensor were discussed. As shown in Fig. S8A, when *E. coli* and *P. aeruginosa* were detected, there were no significant changes of peak current values between different concentrations, while the peak current values of *S. aureus* changed significantly with the change of concentrations. This can be attributed to the specific adsorption between antigens and antibodies. And the result suggested that this immunosensor had a high selectivity. In order to research the stability of the developed immunosensor, the peak current values were recorded periodically. The immunosensor was stored in PBS (pH = 7.4) at 4 °C when it was not in use. The current response dropped less than 10% of its initial response after storing for a month. These results suggested that the developed immunosensor was long-term stable (Fig. S8B). The reproducibility of the proposed immunosensor was investigated by monitoring the current signals in the presence of $1*10^4$ CFU/mL *S. aureus* for five electrodes under the same conditions (Fig. S8C). The relative standard deviation (RSD) for *S. aureus* was found to be 4.84%, which was reasonable for the sensing platform.

3.9. Analytical application of the immunosensor in real samples

To test the feasibility of the immunosensor for the detection of *S. aureus*, it was applied to water samples containing different concerntrations of *S. aureus* (Table 1). The results obtained by this immunosensor were consistent with the results got by the plate counting method, indicating acceptable precision.

In view of the excellent anti-biofouling property of Ab@S-HA@MMSNs/MGCE, it was also applied for detecting *S. aureus* in the whole blood. The calibration plot for *S. aureus* detection in whole blood was shown in Fig. S6. The regression equation was ΔI (10^{-6} A) = -0.2348 logC(CFU/mL)-0.8292 (R^2 = 0.9665) and the detection limit was 5 CFU/mL based on signals-to-noise ratio (3 S/N), which suggested that the developed immunosensor could be potentially used for the detection of clinical blood samples (Figs. S9A–S9B).

4. Conclusion

In this study, an "on-demand" integrated platform for diagnosis and treatment towards *S. aureus* has been firstly costructed. It showed good blood compatibility and controlled release of van, which ensure that it could be used to kill *S. aureus* in the whole blood. And the Ab@S-HA@MMSNs modified MGCE showed good electrochemical response towards *S. aureus* in the range of $1*10^1$–$1*10^{10}$ CFU/mL with high selectivity, stability and reproducibility. The detection limit was up to 3 CFU/mL, and this responsiveness was also well demonstrated in the blood environment. Therefore, this integrated platform would be a promising multifunctional platform for achieving accurate diagnosis and efficient treatment of *S. aureus* bloodstream infection.

Declaration of competing interest

The authors declare that they have no known competing financial interests or personal relationships that could have appeared to influence the work reported in this paper.

CRediT authorship contribution statement

Tingting Xu: Conceptualization, Methodology, Writing - original draft, Writing - review & editing. **Jiming Li:** Investigation, Data curation. **Shaoyin Zhang:** Investigation, Data curation. **Yongcan Jin:** Resources, Supervision, Validation. **Rui Wang:** Resources, Investigation, Writing - review & editing.Acknowledgements

This work was supported by the National Natural Science Foundation of China (51703095, 31730106), Natural Science Foundation of Jiangsu Province (BK20171010, SBK2017043718) and Nanjing Forestry University 2018 Scientific Research Start-up Funds (163105042).

Conflicts of interest

There are no conflicts of interest.

Appendix A. Supplementary data

Supplementary data to this article can be found online at https://doi.org/10.1016/j.bios.2019.111507.

References

Abatangelo, G., Barbucci, R., Brun, P., Lamponi, S., 1997. Biocompatibility and enzymatic degradation studies on sulphated hyaluronic acid derivatives. Biomaterials 18, 1411–1415.

Barbucci, R., Lamponi, S., Magnani, A., Poletti, L.F., Rhodes, N.P., Sobel, M., Williams, D.F., 1998. Influence of sulfation on platelet aggregation and activation with differentially sulfated hyaluronic acids. J. Thromb. Thrombolysis 6, 109–115.

Bu, T., Huang, Q., Yan, L.Z., Zhang, W.T., Dou, L.N., Huang, L.J., Yang, Q.F., Zhao, B.X., Yang, B.W., Li, T., Wang, J.L., Zhang, D.H., 2019. Applicability of biological dye tracer in strip biosensor for ultrasensitive detection of pathogenic bacteria. Food Chem. 274, 816–821.

Cao, S.W., Zhu, Y.J., Ma, M.Y., Li, L., Zhang, L., 2008. Hierarchically nanostructured magnetic hollow spheres of Fe_3O_4 and γ-Fe_2O_3: preparation and potential application in drug delivery. J. Phys. Chem. C 112, 1851–1856.

Cen, L., Neoh, K.G., Li, Y.L., Kang, E.T., 2004. Assessment of in vitro bioactivity of hyaluronic acid and sulfated hyaluronic acid functionalized electroactive polymer. Biomacromolecules 5, 2238–2246.

Cheng, M., Wang, Z.K., Lv, Q., Li, C.L., Sun, S.Q., Hu, S.Q., 2018. Preparation of amino-functionalized Fe_3O_4@$mSiO_2$ core-shell magnetic nanoparticles and their application for aqueous Fe^{3+} removal. J. Hazard Mater. 341, 198–206.

Chi, Y.C., Xue, J.J., Zhuo, J.K., Zhang, D.H., Liu, M., Yao, Q., 2018. Catalytic co-pyrolysis of cellulose and polypropylene over all-silica mesoporous catalyst MCM-41 and Al-MCM-41. Sci. Total Environ. 633, 1105–1113.

Cooksey, E.M., Singh, G., Scott, L.C., Aw, T.G., 2019. Detection of coliphages and human adenoviruses in a subtropical estuarine lake. Sci. Total Environ. 649, 1514–1521.

Duangkamon, B., Volkhard, H., 2015. Quantitative study of BSA coating silica nanoparticle. J. Math. Chem. 53, 29–40.

Dubourg, G., Lamy, B., Ruimy, R., 2018. Rapid phenotypic methods to improve the diagnosis of bacterial bloodstream infections: meeting the challenge to reduce the time

to result. Clin. Microbiol. Infect. 24, 935–943.
Ferrer, R., Ignacio, M.L., Phillips, G., Osborn, T.M., Townsend, S., Dellinger, R.P., Artigas, A., Schorr, C., Levy, M.M., 2014. Empiric antibiotic treatment reduces mortality in severe sepsis and septic shock from the first hour: results from a guideline-based performance improvement program. Crit. Care Med. 42, 1749–1755.
Guo, S.J., Wen, D., Zhai, Y.M., Dongd, S.J., Wang, E.K., 2010. Platinum nanoparticle ensemble-on-graphene hybrid nanosheet: one-pot, rapid synthesis, and used as new electrode material for electrochemical sensing. ACS Nano 4, 3959–3968.
Han, J., Wang, L., Wang, L., Li, C.M., Mao, Y.L., Wang, Y., 2019. Fabrication of a core-shell-shell magnetic polymeric microsphere with excellent performance for separation and purification of bromelain. Food Chem. 283, 1–10.
Ji, H.W., Dong, K., Yan, Z.Q., Ding, C., Chen, Z.W., Ren, J.S., Qu, X.G., 2016. Bacterial hyaluronidase self-triggered prodrug release for chemo-photothermal synergistic treatment of bacterial infection. Small 12, 6200–6206.
Li, Z.L., Fan, X.L., Liu, J., Hu, Y., Yang, Y.W., Li, Z., Chen, C.Y., Yu, M., 2018. Mesoporous silica-coated bismuth nanohybrids as a new platform for photoacoustic/computed tomography imaging and synergistic chemophotothermal therapy. Nanomedicine 13, 2283–2300.
Liu, M., Yue, X.L., Dai, Z.F., Xing, L., Ma, F., Ren, N.Q., 2007. Stabilized hemocompatible coating of nitinol devices based on photo-cross-linked alginate/heparin multilayer. Langmuir 23, 9378–9385.
Lu, J., Do, I., Drzal, L.T., Worden, R.M., Lee, I., 2008. Nanometal-decorated exfoliated graphite nanoplatelet based glucose biosensors with high sensitivity and fast response. ACS Nano 2, 1825–1832.
Mohammadniaei, M., Yoon, J., Lee, T., Bharate, B.G., Jo, J., Lee, D., Choi, J.W., 2018. Electrochemical biosensor composed of silver ion-mediated dsDNA on Au-encapsulated Bi_2Se_3 nanoparticles for the detection of H_2O_2 released from breast cancer cells. Small 14, 1703970.
Mura, S., Couvreur, P., 2012. Nanotheranostics for personalized medicine. Adv. Drug Deliv. Rev. 64, 1394–1416.
Neto, A.I., Cibrao, A.C., Correia, C.R., Carvalho, R.R., Luz, G.M., Ferrer, G.G., Botelho, G., Picart, C., Alves, N.M., Mano, J.F., 2014. Nanostructured polymeric coatings based on chitosan and dopamine-modified hyaluronic acid for biomedical applications. Small 10, 2459–2469.
Ni, D.L., Bu, W.B., Ehlerding, E.B., Cai, W.B., Shi, J.L., 2017. Engineering of inorganic nanoparticles as magnetic resonance imaging contrast agents. Chem. Soc. Rev. 46, 7438–7468.
Nor, Y.A., Zhang, H.W., Purwajanti, S., Song, H., Meka, A.K., Wang, Y., Mitter, N., Mahony, D., Yu, C.Z., 2016. Hollow mesoporous carbon nanocarriers for vancomycin delivery: understanding the structure–release relationship for prolonged antibacterial performance. J. Mater. Chem. B 4, 7014–7021.
Ranjbar, S., Shahrokhian, S., 2018. Design and fabrication of an electrochemical aptasensor using Au nanoparticles/carbon nanoparticles/cellulose nanofibers nanocomposite for rapid and sensitive detection of *Staphylococcus aureus*. Bioelectrochemistry 123, 70–76.
Rubab, M., Shahbaz, H.M., Olaimat, A.N., Oh, D.H., 2018. Biosensors for rapid and sensitive detection of Staphylococcus aureus in food. Biosens. Bioelectron. 105, 49–57.
Smith, B.S., Yoriya, S., Grissom, L., Grimes, C.A., Popat, K.C., 2010. Hemocompatibility of titania nanotube arrays. J. Biomed. Mater. A 95A, 350–360.
Sun, C., Liu, Y.L., Tong, F.Y., Mao, C., Huang, X.H., Zhao, B., Shen, J., 2013. Preparation of novel electrochemical glucose biosensors for whole blood based on antibiofouling polyurethane-heparin nanoparticles. Electrochim. Acta 97, 349–356.
Sun, P.P., Zhang, Y., Ran, X., Liu, C.Y., Wang, Z.Z., Ren, J.S., Qu, X.G., 2018. Phytochemical-encapsulated nanoplatform for “on-demand” synergistic treatment of multidrug-resistant bacteria. Nano Res 11, 3762–3770.
Thammavongsa, V., Kim, H.K., Missiakas, D., Schneewind, O., 2015. Staphylococcal manipulation of host immune responses. Nat. Rev. Microbiol. 13, 529–543.
Thiangthan, S., Runt, J., Manuspiya, H., 2019. Sulfonation of dialdehyde cellulose extracted from sugarcane bagasse for synergistically enhanced water solubility. Carbohydr. Polym. 208, 314–322.
Tong, F.Y., Chen, X.Q., chen, L.B., zhu, P.Y., Luan, J.F., Mao, C., Bao, J.C., Shen, J., 2013. Preparation, blood compatibility and anticoagulant effect of heparin-loaded polyurethane microspheres. J. Mater. Chem. B 1, 447–453.
Tucking, K.S., Vasani, R.B., Cavallaro, A.A., Voelcker, N.H., Schonherr, H., Prieto, S.B., 2018. Hyaluronic acid–modified porous silicon films for the electrochemical sensing of bacterial hyaluronidase. Macromol. Rapid Commun. 39, 1800178.
Wang, J.H., Zheng, S.R., Shao, Y., Liu, J.L., Xu, Z.Y., Zhu, D.Q., 2010. Amino-functionalized Fe_3O_4@SiO_2 core–shell magnetic nanomaterial as a novel adsorbent for aqueous heavy metals removal. J. Colloid Interface Sci. 349, 293–299.
Wang, R., Li, J.Z., Chen, W., Xu, T.T., Yun, S.F., Xu, Z., Xu, Z.Q., Sato, T., Chi, B., Xu, H., 2017. A Biomimetic mussel-inspired ε-poly-l-lysine hydrogel with robust tissue-anchor and anti-infection capacity. Adv. Funct. Mater. 27, 1604894.
Xu, T.T., Chi, B., Wu, F., Ma, S.S., Zhan, S.Y., Yi, M.H., Xu, H., Mao, C., 2017. A sensitive label-free immunosensor for detection α-Fetoprotein in whole blood based on anticoagulating magnetic nanoparticles. Biosens. Bioelectron. 95, 87–93.
Yang, P.P., Quan, Z.W., Hou, Z.Y., Li, C.X., Kang, X.J., Cheng, Z.Y., Lin, J., 2009. A magnetic, luminescent and mesoporous core–shell structured composite material as drug carrier. Biomaterials 30, 4786–4795.
Yao, X.X., Niu, X.X., Ma, K.X., Huang, P., Grothe, J., Kaskel, S., Zhu, Y.F., 2017. Graphene quantum dots-capped magnetic mesoporous silica nanoparticles as a multifunctional platform for controlled drug delivery, magnetic hyperthermia, and photothermal therapy. Small 13, 1602225.
Yu, T., Malugin, A., Ghandehari, H., 2011. Impact of silica nanoparticle design on cellular toxicity and hemolytic activity. ACS Nano 5, 5717–5728.
Yuan, Y., Ni, X.J., Cao, Y.H., 2016. Electrochemical determination of hemoglobin on a magnetic electrode modified with chitosan based on electrocatalysis of oxygen. J. Electroanal. Chem. 837, 219–225.
Zhang, X., Thavasi, V., Mhaisalkar, S.G., Ramakrishna, S., 2012. Novel hollow mesoporous 1D TiO_2 nanofibers as photovoltaic and photocatalytic materials. Nanoscale 5, 1707–1716.
Zheng, X.L., Ge, J.C., Wu, J.S., Liu, W.M., Guo, L., Jia, Q.Y., Ding, Y., Zhang, H.Y., Wang, P.F., 2018a. Biodegradable hypocrellin derivative nanovesicle as a near-infrared light-driven theranostic for dually photoactive cancer imaging and therapy. Biomaterials 185, 133–141.
Zheng, G.R., Zhao, R.R., Xu, A.X., Shen, Z.C., Chen, X., Shao, J.W., 2018b. Co-delivery of sorafenib and siVEGF based on mesoporous silica nanoparticles for ASGPR mediated targeted HCC therapy. Eur. J. Pharm. Sci. 111, 492–502.